

1 Running head: Selenium and ecological partnerships in *Astragalus*

2

3 Author for correspondence: Elizabeth A. H. Pilon-Smits, Biology Department, Colorado State

4 University, Fort Collins, CO 80523, USA; Tel: 970-491-4991; Email: epsmits@lamar.colostate.edu

5

6 Journal area more appropriate for the paper: Plants Interacting with Other Organisms

7

8

9 **Selenium distribution and speciation in hyperaccumulator *Astragalus bisulcatus***
10 **and associated ecological partners**

11

12 José R. Valdez Barillas^{1,2)*}, Colin F. Quinn^{1)*}, John L. Freeman^{1,3,4)*}, Stormy D. Lindblom¹⁾,
13 Sirine C. Fakra⁵⁾, Matthew A. Marcus⁵⁾, Todd M. Gilligan⁶⁾, Élan R. Alford⁷⁾,
14 Ami L. Wangeline⁸⁾, and Elizabeth A.H. Pilon-Smits¹⁾

15

16 ¹⁾ Biology Department, Colorado State University, Fort Collins, CO 80523, USA

17 ²⁾ Biology Department, Texas A&M University-San Antonio, San Antonio, TX 78224, USA

18 ³⁾ California State University Fresno, Department of Biology, Fresno CA 93740, USA,

19 ⁴⁾ California State University Fresno, Center for Irrigation Technology, Fresno CA, 93740

20 ⁵⁾ Advanced Light Source, Lawrence Berkeley National Laboratory, Berkeley, CA 94720, USA

21 ⁶⁾ Department of Bioagricultural Sciences and Pest Management, Colorado State University, Fort
22 Collins, CO 80523, USA

23 ⁷⁾ Department of Forest and Rangeland Stewardship, Colorado State University, Fort Collins, CO
24 80523, USA

25 ⁸⁾ Department of Biology, Laramie County Community College, Cheyenne, WY 82007, USA

26

27 * Authors contributed equally to this manuscript

28

29 Footnotes:

30

31 Funding for these studies was provided by National Science Foundation grant # IOS-0817748 to
32 EAHPS. The Advanced Light Source is supported by the Office of Science, Basic Energy
33 Sciences, and Division of Materials Science of the U.S. Department of Energy (DE-AC02-
34 05CH11231).

35

36 Corresponding author: Elizabeth A. H. Pilon-Smits, epsmits@lamar.colostate.edu

37 **ABSTRACT**

38 The goal of this study was to investigate how plant selenium (Se) hyperaccumulation may affect
39 ecological interactions, and whether associated partners may affect Se hyperaccumulation. The Se
40 hyperaccumulator *Astragalus bisulcatus* was collected in its natural seleniferous habitat, and X-ray
41 fluorescence mapping and X-ray absorption near-edge structure spectroscopy were used to
42 characterize Se distribution and speciation in all organs, as well as in encountered microbial
43 symbionts and herbivores. Selenium was present at high levels (704 - 4,661 mg kg⁻¹ DW) in all
44 organs, mainly as organic C-Se-C compound(s) (i.e. Se bonded to two organic groups)
45 indistinguishable from methyl-selenocysteine. In nodules, root and stem, up to 34% of Se was
46 found as elemental Se, which was potentially due to microbial activity. In addition to a nitrogen-
47 fixing symbiont, the plants harbored an endophytic fungus that produced elemental Se.
48 Furthermore, two Se-resistant herbivorous moths were discovered on *A. bisulcatus*, one of which
49 was parasitized by a wasp. Adult moths, larvae and wasp all accumulated predominantly C-Se-C
50 compounds. In conclusion, hyperaccumulators live in association with a variety of Se-resistant
51 ecological partners. Among these partners, microbial endosymbionts may affect Se speciation in
52 hyperaccumulators. Hyperaccumulators have been shown earlier to negatively affect Se-sensitive
53 ecological partners, while apparently offering a niche for Se-resistant partners. Through their
54 positive and negative effects on different ecological partners, hyperaccumulators may influence
55 species composition and Se cycling in seleniferous ecosystems.

56

57 **INTRODUCTION**

58

59 Selenium (Se) hyperaccumulation in plants is an evolutionary adaptation that facilitates the
60 accumulation of Se to levels in excess of 0.1% of plant dry weight (DW), or >1,000 mg Se kg⁻¹
61 DW (Beath *et al.*, 1939a,b). An extreme example is *Astragalus bisulcatus* (two-grooved
62 milkvetch), which is capable of accumulating Se to levels up to 15,000 mg Se kg⁻¹ DW (Galeas *et al.*,
63 2007). Like other hyperaccumulators, populations of *A. bisulcatus* are almost exclusively
64 found on seleniferous soils, where Se levels may range from 1-100 mg Se kg⁻¹ soil (Beath *et al.*,
65 1939a,b).

66 Selenium is thought to be taken up by plants mainly as selenate (SeO₄²⁻, the predominant
67 form of bioavailable Se in soils) via sulfate transporters, and reduced and incorporated into
68 selenoaminoacids by the sulfur assimilation pathway (for reviews see Sors *et al.*, 2005; Pilon-
69 Smits and Quinn, 2010). Selenate is reduced to selenite (SeO₃²⁻), and then to selenide (Se²⁻), which
70 is incorporated into selenocysteine (SeCys). The non-specific incorporation of SeCys into proteins
71 is presumed to be toxic (Stadtman, 1990). Selenium hyperaccumulators avoid Se toxicity by
72 methylating SeCys to methyl-selenocysteine (MeSeCys) via a unique enzyme, selenocysteine
73 methyltransferase (SMT), effectively circumventing the misincorporation of SeCys into protein
74 (Neuhierl and Böck, 1996).

75 Micro-focused X-ray fluorescence (μXRF) mapping and Se K-edge X-ray absorption near-
76 edge structure (μXANES) have previously been utilized to investigate the spatial distribution and
77 chemical speciation of Se in hyperaccumulator leaves (Freeman *et al.*, 2006a). While non-
78 hyperaccumulator plants were found to accumulate Se primarily in the leaves as selenate (de Souza
79 *et al.*, 1998), Se hyperaccumulators accumulate Se predominantly in the leaf epidermis in organic
80 forms with a C-Se-C configuration, i.e. Se bonded to two organic groups (Freeman *et al.*, 2006a).
81 *A. bisulcatus* showed specific Se sequestration in the leaf trichomes, in the form of C-Se-C
82 compounds that were identified as MeSeCys and γ-glutamylmethylselenocysteine using liquid
83 chromatography – mass spectroscopy (Freeman *et al.*, 2006a).

84 Selenium hyperaccumulators exhibit variability in Se hyperaccumulation throughout the
85 growing season and between different organs. Seasonal fluctuations in Se hyperaccumulation
86 were observed in a field study of *A. bisulcatus* (Galeas *et al.*, 2007). During the spring, Se

87 appeared to be translocated from the root to the emerging leaves, reaching maximum levels in mid-
88 spring. Leaf Se levels then dropped gradually during summer and fall and rose in reproductive
89 organs and roots as Se was presumably remobilized from the leaves to reproductive organs and
90 back into the roots during shoot senescence. The form of Se that is remobilized may be organic, as
91 *A. bisulcatus* was shown to accumulate mostly organic Se in young leaves and roots, while older
92 leaves hyperaccumulated mainly inorganic selenate and at much lower concentrations (Pickering *et*
93 *al.*, 2000).

94 The functional significance of Se hyperaccumulation and the ecological implications of the
95 extreme Se levels have been a topic of recent interest. Several studies suggest that Se
96 hyperaccumulation has evolved as a defense mechanism against herbivory. Selenium can protect
97 plants from a wide variety of Se-sensitive invertebrate and vertebrate herbivores, due to deterrence
98 and toxicity (for reviews see Quinn *et al.*, 2007; Boyd, 2007, 2010; El Mehdawi and Pilon-Smits,
99 2012). Selenium has been shown to protect plants from aphids (Hurd-Karrer and Poos, 1936;
100 Hanson *et al.*, 2004), moth and butterfly larvae (Vickerman *et al.*, 2002; Hanson *et al.*, 2003;
101 Freeman *et al.*, 2006b), crickets and grasshoppers (Freeman *et al.*, 2007), thrips and spider mites
102 (Quinn *et al.*, 2010), and prairie dogs (Quinn *et al.*, 2008; Freeman *et al.*, 2009). The
103 hyperaccumulators *A. bisulcatus* and *Stanleya pinnata* also harbored fewer arthropods in their
104 native seleniferous habitat when compared to adjacent non-hyperaccumulators (Galeas *et al.*,
105 2008).

106 Hyperaccumulator plants may host Se-tolerant herbivores, as shown in a previous study
107 which reported a Se-tolerant moth species associated with *S. pinnata* (Freeman *et al.*, 2006b).
108 Larvae from a population of Se-tolerant *Plutellidae* closely resembling the diamondback moth
109 (*Plutella xylostella*), a damaging agricultural pest, were collected from *S. pinnata* in a seleniferous
110 area (Fort Collins, CO, U.S.A.). These larvae were documented through laboratory tests to tolerate
111 the hyperaccumulated Se (2,000 mg kg⁻¹ DW) in *S. pinnata* leaves, and not to be deterred by high-
112 Se plants. In contrast, a diamondback moth population collected and reared from a non-
113 seleniferous area in the Eastern U.S.A. quickly died after feeding on high-Se leaves and was
114 deterred by high-Se *S. pinnata* plants (Freeman *et al.*, 2006b). A potential mechanism for the
115 difference in Se tolerance between the two moth populations was revealed by Se K-edge XANES
116 and liquid chromatographic mass spectroscopy (LCMS) analyses, which demonstrated that the Se-

117 tolerant moth accumulated MeSeCys, similar to its host plant *S. pinnata*, while the Se-sensitive
118 population accumulated SeCys and had obvious disintegration of internal organs (Freeman *et al.*,
119 2006b). Selenocysteine is considered more toxic to organisms than MeSeCys, due to its non-
120 specific incorporation into proteins in the place of cysteine; the resulting absence of disulfide
121 bonds crucially affects protein structure and function (Stadtman, 1990). The same study by
122 Freeman *et al.* (2006b) characterized a biochemical flux of Se into a higher trophic level because
123 the Se-tolerant moth larvae were actively parasitized by the microgastrine wasp *Diadegma*
124 *insulare* (Braconidae), which also accumulated C-Se-C forms, mainly as MeSeCys.

125 In addition to protecting plants from generalist herbivores, accumulated Se may offer
126 protection from Se-sensitive microbial plant pathogens. *Brassica juncea* (Indian mustard) plants
127 treated with Se were less susceptible to a fungal leaf pathogen (*Alternaria brassicicola*) and a
128 fungal root/stem pathogen (*Fusarium sp.*), compared to control plants not supplemented with Se
129 (Hanson *et al.*, 2003). On the other hand, it appears that a variety of Se-tolerant microbes live in
130 association with hyperaccumulators. A litter decomposition study conducted on seleniferous soil
131 showed that native *A. bisulcatus* litter naturally high in Se decomposed faster and harbored higher
132 numbers of microbes and micro-arthropods than low-Se *Medicago sativa* litter collected in the
133 same area (Quinn *et al.*, 2011a). Furthermore, Se-tolerant fungi were isolated from the rhizosphere
134 of hyperaccumulators *A. bisulcatus* and *S. pinnata* (Wangeline and Reeves, 2007), and rhizosphere
135 fungi from hyperaccumulators growing on seleniferous soil were significantly more Se-tolerant
136 than fungi from non-seleniferous areas (Wangeline *et al.*, 2011).

137 The effects of hyperaccumulation have also been studied in relation to plant-to-plant
138 interactions. El Mehdawi *et al.* (2011a) observed that soil around *A. bisulcatus* and *S. pinnata*
139 hyperaccumulators in the field was enriched in Se, and this high-Se soil could significantly impair
140 germination and growth of Se-sensitive plants. Thus, Se hyperaccumulation may function as a
141 form of elemental allelopathy against Se-sensitive neighbors. On the other hand, some apparently
142 Se-resistant neighbors of Se hyperaccumulators were found to benefit from their enhanced Se
143 levels around hyperaccumulators. When *Symphyotrichum ericoides* (white heath aster) and
144 *Artemisia ludoviciana* (white sage brush) were growing next to hyperaccumulators they contained
145 10-20 fold higher Se concentrations ($>1,000$ mg Se kg^{-1} DW), were 2-times larger, and had

146 reduced herbivore loads and less herbivory damage compared to plants from the same species that
147 were not growing next to hyperaccumulators (El Mehdawi *et al.*, 2011b).

148 In order to better characterize Se distribution and speciation in *A. bisulcatus* we used μ XRF
149 elemental mapping and Se K-edge μ XANES to characterize the Se distribution and speciation in
150 all organs of mature *A. bisulcatus*, as well as in seeds and seedlings. In addition, we studied the Se
151 distribution and speciation in several below- and above-ground ecological partners of *A.*
152 *bisulcatus*. The objectives of this study were to present an in-depth analysis of the Se distribution
153 across different organs of a hyperaccumulator and to obtain better insight into how Se
154 hyperaccumulation affects ecological interactions and how ecological partners may affect Se
155 hyperaccumulation.

156

157 **RESULTS**

158 **Total Se and S concentration in different *A. bisulcatus* plant parts**

159 The *A. bisulcatus* plants collected in the field hyperaccumulated Se to concentrations ranging from
160 704 – 4,661 mg kg⁻¹ DW in different organs (Table I). The highest Se concentrations were
161 measured in the flowers, followed by stems, leaves, and roots with a 1.5-fold difference between
162 flowers and leaves and a 6.5-fold difference between flowers and roots ($t=3.06$, $P < 0.05$). Within
163 *A. bisulcatus* flowers the highest Se level was measured in the sepals and petals, followed by
164 pistils and stamens; immature seeds collected from developing seed pods had an intermediate Se
165 level (Table I). Since Se is chemically similar to sulfur (S) and thought to be transported and
166 metabolized via the same molecular machinery, tissue S concentration was also analyzed for
167 comparison. Sulfur levels were highest in leaves, followed by flowers, stems and roots ($F_{3,8} =$
168 17.10, $P < 0.001$, Table I). In the floral parts the S concentrations were higher in sepals and petals
169 than in stamens or pistils, and were the highest in immature seeds (Table I).

170 **Distribution and speciation of Se in different plant parts and ecological partners**

171 Roots and nodules

172 The distribution of Se in the upper portion of the tap root from a field-collected *A. bisulcatus* (Fig.
173 1A) was fairly homogeneous as shown by μ XRF, with a higher Se signal in the cortex and stele

174 than in the periderm (perimeter). Micro XANES analysis of Se in the cortex of the taproot
175 demonstrated 89% was in an organic C-Se-C form. This C-Se-C may be methyl-SeCys,
176 γ GluMeSeCys, SeCysth and/or SeMet, since the XANES spectra for these compounds are virtually
177 indistinguishable. The remaining 11% of the Se in the upper tap root was detected as elemental Se
178 (Se^0) (Fig. 1B).

179 In the smaller, lateral roots the strongest Se signal was found at the tip and along the
180 periphery of the root, likely the epidermis (Fig. 1C). There was an equally strong Se signal in the
181 associated nodule (Fig. 1C). Interestingly, there was a clear difference in Se speciation between
182 the root and the nodule. In the root Se was 100% C-Se-C (Fig. 1C white circles and Fig. 1D), while
183 in the nodule 46% was C-Se-C, 31% Se^0 and 23% selenite (Fig. 1C black circles and Fig. 1E).

184 Stems and leaves

185 In the (hollow) woody stem of *A. bisulcatus* Se was localized throughout the cortex (Fig. 2A).
186 Within the cortex there is not enough resolution to distinguish vascular tissue from ground tissue,
187 but some of the more Se-rich spots appear to be arranged in a ring, which is best visible along the
188 top right of the image, and may correspond with vascular bundles. The rim along the outside of the
189 cross-section is also particularly elevated in Se (best visible on the lower left) and likely
190 corresponds with the epidermis (Fig. 2A). In the cortex Se was detected as 50% C-Se-C, 31% Se^0
191 and 16% selenite (Fig. 2B). Leaves of *A. bisulcatus* concentrated Se to extreme levels in downy
192 trichomes (Fig. 2C, as previously reported, Freeman *et al.*, 2006a). An estimated 70 % of total leaf
193 Se was located in trichomes, predominantly (98%) in the form of C-Se-C, consisting of the two
194 compounds MeSeCys and γ GluMeSeCys, as identified by LC-MS (Fig. 2D). The remaining 30%
195 of the total leaf Se, outside of the trichomes, consisted of 70% C-Se-C, 20% selenate and 10%
196 selenite. When these two fractions were combined, the entire leaf was estimated to contain 91% C-
197 Se-C, 6% selenate and 3% selenite (Fig. 2D, Freeman *et al.*, 2006a). Here it is worth mentioning
198 that speciation fractions below 10% should be interpreted with caution because of the error margin
199 of the least square linear combination (LSQ) analysis of Se XANES spectra.

200 Leaf herbivores

201 Larvae of two different moth species were found feeding – and apparently thriving - on leaves of
202 *A. bisulcatus* in the field. The first species, collected during late summer, was identified using

203 PCR as *Apamea sordens* (Hufnagel) (Noctuideae). The larva of *A. sordens* was shown by μ XRF
204 mapping to accumulate Se in the anterior head lobes (vertex), the lateral portion of the abdomen
205 (spiracular band), and the hindgut (Fig. 3A). The vertex and the spiracular band contained 96%
206 organic C-Se-C (Fig. 3A, white circles, Fig. 3B). The hindgut contained 76% C-Se-C and 24%
207 selenate (Fig. 3A, white circle, Fig. 3C). Larvae collected from the field were allowed to pupate,
208 and the emerging adult (pictured in Fig. 3D) was mapped for Se accumulation by μ XRF. It
209 accumulated Se preferentially in the lower abdomen and the hindgut (Fig. 3E). Micro XANES
210 analysis demonstrated that Se in the lower abdomen and hindgut consisted of 76% C-Se-C, 20%
211 Se^0 and 4% selenite (Fig. 3F). Some of the *A. sordens* larvae collected in the field hatched a
212 parasitoid wasp that was identified based on morphology to be in the family Ichneumonidae,
213 subfamily Cryptinae (Fig. 3G). Micro XRF mapping of this wasp showed a substantial Se signal
214 in the head, thorax and abdomen (Fig. 3H). Se XANES analyses of the head and abdomen
215 demonstrated that 78% of the total Se was C-Se-C, 12% was seleno-diglutathione and 10% selenite
216 (Fig. 3I). The thorax differed in that it contained relatively less C-Se-C (59%), and more Se^0
217 (26%) and selenite (15%) (Fig. 3J).

218 A second moth species (Fig. 4A, D) was observed feeding on *A. bisulcatus* in the late
219 summer and early fall. This moth was collected and tentatively identified as belonging to the
220 family Gelechiidae, based on the upcurved labial palpi (mouthparts) of the adult and the overall
221 morphology of the adult and larva. Micro XRF mapping showed that Se was present throughout
222 the larval and adult tissues, with a stronger concentration in what appears to be the digestive tract
223 (Fig. 4B, D). Micro XANES analyses showed that Se was present as organic forms with a C-Se-C
224 configuration (98-100%) in both larva and adult, and both in the animal tissues and in the apparent
225 digestive tract (Fig. 4C, F).

226 Flowers

227 The *A. bisulcatus* flower (Fig. 5A) was shown by μ XRF to contain Se in the petals (Fig. 5B) as
228 well as in the pistil and stamen (Fig. 5C). Within the petals and pistil Se appears to be distributed
229 fairly homogeneously, with a slight concentration in the ovules (Fig. 5B, C). The anthers show a
230 strong Se signal at the base, as well as in apparent vascular tissue connecting the base with the

231 anther. Selenium speciation was similar in the different flower parts, averaging 90% C-Se-C, 7%
232 Se⁰ and 3% selenite (Fig. 5D).

233

234 Seeds, seedlings, and a seed endosymbiont

235 The seeds of *A. bisulcatus* (Fig. 6A) concentrated Se in the embryo and not in the seed coat (Fig.
236 6B). The form of Se was almost exclusively organic, with a C-Se-C configuration (Fig. 6C).
237 Surface-sterilized seeds of *A. bisulcatus* showed evidence of an endophytic fungus, which
238 appeared in more than 50% of the germinating surface-sterilized seeds (Fig. 6D). Based on
239 morphology and internal transcribed spacer (ITS) sequence (data not shown) it was identified as a
240 small-spored filamentous fungus belonging to the genus *Alternaria*. Micro XRF analysis
241 demonstrated Se accumulation in the fungal hyphae that emerged from the seeds (Fig. 6E). The Se
242 in the mycelia consisted of 59% C-Se-C, 22% Se⁰ and 19% selenite (Fig. 6F). The cotyledons of
243 the infected seed embryo contained 74% C-Se-C, 20% Se⁰ and 6% selenite (Fig. 6G). Thus, the
244 fungus-infected seedling contained relatively less organic and more inorganic Se compared to the
245 seed proper, and the fungus-infected seed contained relatively more inorganic Se than the
246 uninfected seed. Uninfected seeds and cotyledons showed little or no elemental Se⁰.

247 In order to investigate the movement and biochemical transformation of Se in seedlings, *A.*
248 *bisulcatus* seeds were germinated on selenate-containing growth medium and the resulting
249 seedlings flash-frozen for XAS analysis at two different time points after germination. The mature
250 seedling pictured in Fig. 7A represents the last harvested seedling at day five after germination.
251 Micro XRF mapping demonstrated that *A. bisulcatus* had a fairly uniform distribution of Se in
252 seedling cotyledons, hypocotyls and roots, including root hairs (Fig. 7B). Twenty-four hours
253 following germination the seedling contained 100% C-Se-C in cotyledons and root (Fig. 7B; note:
254 the root tip was desiccated during the XAS analysis). Five days following germination, the
255 cotyledon (Fig. 7C, white circle) contained 95% C-Se-C and 5% selenite, while the root contained
256 relatively less C-Se-C (70%) and a substantial fraction of inorganic Se: 18% Se⁰ and 12% selenite
257 (Fig. 7C, black circle).

258

259 **DISCUSSION**

260 Our survey of Se distribution and speciation in different organs of Se hyperaccumulator *A.*
261 *bisulcatus* demonstrates that Se speciation varies between organs, as summarized in Figure 8.
262 Particularly interesting was the finding that *A. bisulcatus* roots, nodules, stems and flowers
263 contained a substantial fraction of elemental Se, up to 34% Se⁰, a novel finding for plants. Since
264 Se⁰ is produced by many fungi and bacteria, the Se⁰ found here may be a chemical signature from
265 microbial detoxification inside the plant, derived from endophytic microbial partners. These results
266 build on an earlier study by Freeman et al. (2006a) but are novel because in the earlier study only
267 the leaf of *A. bisulcatus* was analyzed, and no elemental Se was found. Here we analyzed all
268 organs, and found significant levels of Se⁰ in several of them. The current study also provides
269 novel information about Se-resistant microbial and insect ecological partners of *A. bisulcatus*, and
270 their respective Se distribution and speciation patterns (Fig. 8). The picture that emerges from
271 these -as well as earlier- studies is that Se hyperaccumulators live in association with a variety of
272 Se-resistant ecological partners.

273 The predominant form of Se in all *A. bisulcatus* organs was organic Se with a C-Se-C
274 configuration (Fig. 8). The finding that *A. bisulcatus* roots contain mainly C-Se-C is in agreement
275 with a study by Pickering *et al.* (2000), who reported that Se was mainly present in organic form in
276 *A. bisulcatus* roots. For comparison, non-hyperaccumulators *Brassica juncea* (Indian mustard) and
277 *Triticum aestivum* (wheat) accumulated predominantly selenate in their roots when supplied with
278 selenate (Pilon-Smits *et al.*, 1999; Li *et al.*, 2008). At the whole-plant level, *A. bisulcatus* appeared
279 to preferentially accumulate Se in its reproductive tissues; the same pattern was observed for the
280 Se hyperaccumulator *S. pinnata*, but not for non-accumulator *B. juncea* which had higher levels in
281 leaves than in reproductive organs (Quinn *et al.*, 2011b). While the form of Se in flowers was 90%
282 C-Se-C for both *A. bisulcatus* and *S. pinnata*, the Se distribution within flowers was somewhat
283 different for the two hyperaccumulator species (Quinn *et al.*, 2011b). In *A. bisulcatus* the Se
284 concentration was higher in the petals and sepals than in the stamen and pistil, while in *S. pinnata*
285 the opposite pattern was observed. Within the pistil, Se was highly concentrated in the ovules in *S.*
286 *pinnata* (Quinn *et al.*, 2011b), and although a similar trend was visible in *A. bisulcatus* Se was
287 distributed more homogeneously throughout the pistil. Furthermore, in anthers of *A. bisulcatus* Se

288 was concentrated at the base and in apparent vascular tissue, while in *S. pinnata* anthers Se was
289 highly concentrated in the pollen (Quinn *et al.*, 2011b).

290 In addition to organic C-Se-C, *A. bisulcatus* roots, nodules, stems and flowers contained up
291 to 34% Se⁰. Elemental Se is not typically found in plants, although plants have been shown to
292 contain SeCys lyase activity, which can produce elemental Se (Pilon-Smits *et al.* 2002). In contrast
293 to plants, Se⁰ is produced widely by fungi and bacteria (Gharieb *et al.*, 1995; Losi and
294 Frankenberger, 1997). Since Se⁰ is insoluble and less toxic than many other forms of Se, many
295 microbes produce Se⁰ as a means of Se tolerance, either via reduction of selenate or selenite, or by
296 SeCys lyase activity (Sarles *et al.*, 1935; Losi and Frankenberger, 1997; Hunter and Kuykendall,
297 2007). Thus, the Se⁰ found in these field-collected *A. bisulcatus* plants may result from the activity
298 of microbial endosymbionts. A recent study by Lindblom *et al.* (2012) suggests an environmental
299 influence on Se speciation in roots of Se hyperaccumulators: *A. bisulcatus* and *S. pinnata* roots
300 collected in the field contained up to 35% Se⁰, but greenhouse-grown plants from the same two
301 species contained almost exclusively C-Se-C. Moreover, several root-associated fungi isolated
302 from Se hyperaccumulators were shown to accumulate high levels of Se⁰ (Lindblom *et al.*, 2012).
303 The current study provides some indication that microbial symbionts of *A. bisulcatus* may be
304 responsible for the observed Se⁰ in the plant tissues. The root nodule, site of a nitrogen-fixing
305 bacterial endosymbiont, was one of the structures that had a very high Se⁰ fraction (31%), which
306 was around three times higher than in the root itself. Furthermore, a fungal seed endophyte
307 (*Alternaria sp.*) was shown to accumulate a large fraction of the Se in its mycelia in the form of
308 Se⁰ while growing on an *A. bisulcatus* seed; within the infected seed there was also a substantial
309 (although somewhat lower) Se⁰ fraction, but an uninfected seed and a 24h old seedling contained
310 exclusively C-Se-C. An *Alternaria sp.* endophyte could be isolated from surface-sterilized stem
311 and root explants cultivated on fungal growth medium. Considering the life cycle and host
312 colonization of vertically transmitted fungal endophytes, it is possible that the same endophyte
313 occurs throughout the plant. Systemic endophytic colonization in the apoplast of leaves, stems and
314 reproductive structures has been documented for several *Astragalus* species (Ralphs *et al.*, 2008).
315 If this is the case here, it may explain the occurrence of Se⁰ in the seedling root, the tap root and
316 particularly the stem.

317 The strength of the XRF Se signal from the fungal mycelia on the infected seed was similar
318 to that obtained from the root and other plant organs. This suggests that this fungal endophyte is
319 quite Se-tolerant. For comparison, two fungal pathogens (*Alternaria brassicicola* and *Fusarium*
320 *sp.*) were shown earlier to be 50% inhibited in growth on medium with 50 mg Se kg⁻¹ DW, and Se
321 accumulation effectively protected plants against these pathogens (Hanson *et al.*, 2003). In a recent
322 study by Wangeline *et al.* (2011), the growth of an *Aspergillus leporis* strain isolated from the
323 rhizosphere of a non-hyperaccumulator plant growing in a non-seleniferous habitat was reduced by
324 50% when exposed to 30 mg Se L⁻¹, while the growth of another strain of *A. leporis* isolated from
325 the rhizosphere of a hyperaccumulator plant growing in seleniferous habitat was tolerant and
326 actually showed improved by Se in media growth at levels up to 1,000 mg Se L⁻¹. Thus, fungi
327 associated with Se hyperaccumulators, like this seed endosymbiont, may have relatively high Se
328 tolerance.

329 *Astragalus* hyperaccumulators have been reported earlier to host bacteria that can nodulate
330 other, non-hyperaccumulator *Astragalus* species (Wilson and Chin, 1947). The finding that *A.*
331 *bisulcatus* harbored root nodules shows that that *A. bisulcatus* has a nitrogen-fixing bacterial
332 endosymbiont, and the fact that the Se signal intensity in the nodule was similar to that in the root
333 suggests this bacterium is resistant to substantial Se levels. Other Rhizobiaceae have been shown
334 before to differ in Se sensitivity. For example, nodulation and nitrogen fixation in the non-
335 hyperaccumulator *Melilotus indica* were reduced by Se at 1 mg L⁻¹ selenate, which may suggest
336 that the plant and/or bacterial symbiont are Se-sensitive (Wu *et al.*, 1994). On the other hand,
337 some Rhizobiaceae could grow on media with 100 mM selenate or selenite (8,000 mg Se L⁻¹) on
338 which they formed red colonies, indicative of the presence of elemental Se⁰ (Kinkle *et al.*, 1994;
339 Hunter and Kuykendall, 2007). These species (*Rhizobium selenireducens*, *Sinorhizobium fredii*,
340 and *S. meliloti*) are not known to nodulate *Astragalus* species, but it is feasible that the nitrogen-
341 fixing symbiont in *A. bisulcatus* nodules can produce Se⁰. It may be interesting in future
342 investigations to compare the Se tolerance of this hyperaccumulator endosymbiont (if culturable)
343 with that of other rhizobia. If the bacterial endosymbiont of *A. bisulcatus* has unusually high Se
344 tolerance it may have evolved this under the influence of Se in the roots of its hyperaccumulator
345 host. Another interesting aspect of this nitrogen fixing symbiosis is that it may play a role in plant
346 Se hyperaccumulation. The Se-containing amino acid MeSeCys and di-aminoacid γ -glutamyl-

347 MeSeCys are vital components of Se tolerance in *A. bisulcatus* (Sors *et al.*, 2005) as the main
348 forms of Se stored in leaves (Freeman *et al.*, 2006a). The microbial symbiont may provide *A.*
349 *bisulcatus* with a portion of the nitrogen required for the production of these organic
350 selenocompounds.

351 Increased metal tolerance has been reported for rhizospheric partners of several
352 hyperaccumulators, some of which could potentially affect plant metal hyperaccumulation
353 (reviewed in Alford *et al.*, 2010). Similarly, it appears that fungal and bacterial endosymbionts of
354 Se hyperaccumulators have evolved enhanced Se tolerance via their capacity to convert other,
355 more toxic forms of Se to the relatively inert Se⁰ form. These endophytes may not only affect
356 plant Se speciation but also overall plant Se hyperaccumulation and tolerance. This will be an
357 interesting area for further investigations.

358 Other Se-resistant ecological partners of *A. bisulcatus* discovered in this study include two
359 herbivorous moth species and a parasitic wasp. One moth was identified as a member of the
360 Gelechiidae, and the other as *A. sordens*. This is the first record of an *Apamea* species feeding on
361 *A. bisulcatus*. *Apamea sordens* is a medium-sized moth in the family Noctuidae. It is widely
362 distributed across Eurasia from Western Europe to Japan, and also occurs in North America, from
363 British Columbia east to Labrador and south to northeastern Oregon, Colorado and South Carolina
364 (Powell and Opler 2009). Larvae of this species have been reported to feed on Poaceae (Robinson
365 *et al.*, 2010) and are considered to be a pest of wheat, rye, barley, and oat in parts of Eurasia
366 (Grichanov and Ovsyannikova 2009). Lepidoptera species that have been reported to feed on *A.*
367 *bisulcatus* tend to be general Fabaceae feeders and include *Walshia amorphella*
368 (Cosmopterigidae), *Erynnis persius* (Hesperiidae), *Strymon melinus* (Lycaenidae), *Euxoa costata*
369 (Noctuidae), *Colias alexandra* (Pieridae), and *Colias eurytheme* (Pieridae) (Robinson *et al.*, 2010).
370 So far no herbivores have been reported to specialize on *A. bisulcatus*. More studies are needed to
371 determine whether the two moths described here may be specialized feeders on Se
372 hyperaccumulator plants.

373 In the laboratory the capacity of field-collected larvae from both moth species to complete
374 their life cycle on high-Se (>1,000 mg Se kg⁻¹ DW) *A. bisulcatus* plants was confirmed, and based
375 on XRF Se signals the larvae and adults contained substantial Se levels. Thus, both Se-resistant
376 moth herbivores may actually be Se-tolerant, but further studies are needed to investigate this.

377 Both moths accumulated mainly C-Se-C, with smaller fractions as inorganic selenate or Se⁰. The
378 locations where Se⁰ was observed often appeared to correspond with the intestinal tract. It is
379 possible that microbial activity in the intestine of these insects is responsible for the production of
380 the observed Se⁰ in the larvae. The main form of Se in the two moth herbivores described here, C-
381 Se-C, was also shown to accumulate in a Se-tolerant diamondback moth herbivore of
382 hyperaccumulator *S. pinnata* (as MeSeCys, Freeman *et al.*, 2006b). In contrast, a Se-sensitive
383 population of diamondback moth accumulated the apparently de-methylated product SeCys when
384 feeding on *S. pinnata*. Thus, the Se-tolerant diamond-back moth was hypothesized to derive its
385 tolerance from the inability to metabolize the ingested MeSeCys from its hyperaccumulator host.
386 A Se-resistant parasitic wasp of the diamondback moth also accumulated MeSeCys (Freeman *et*
387 *al.*, 2006b). The same mechanism may be responsible for the Se resistance of the two moths and
388 the parasitoid wasp described in this study, since they also accumulated C-Se-C.

389 These parallel findings of Se-resistant moths that feed on different Se hyperaccumulator
390 species, each associated with parasitic wasps suggest Se hyperaccumulators facilitate the evolution
391 of Se-resistant herbivores that can utilize hyperaccumulators as a food source. Such Se-
392 accumulating herbivores may in turn facilitate the evolution of Se-tolerant parasites or predators in
393 higher trophic levels. The accumulation of Se in the larvae and the retention of this Se in the adult
394 may play a role in defending the herbivore against generalist predators and also be a source of Se
395 flux into higher trophic levels. The results from this study complement earlier studies on Se
396 hyperaccumulators (reviewed by El Mehdawi and Pilon-Smits, 2012) and provide further evidence
397 that Se plays a significant role in shaping the ecological interactions of hyperaccumulator plants
398 and in seleniferous ecosystems as a whole. Through their extreme Se concentrations,
399 hyperaccumulator plants may select against Se-sensitive organisms while driving the evolution of
400 Se-tolerant symbiotic partners. Affected organisms may include endophytes, rhizospheric
401 microorganisms, litter detritivores, leaf herbivores, pollinators, parasites, predators, pathogens and
402 neighboring plants. Through positive or negative effects on different ecological partners, Se
403 hyperaccumulators likely have a profound effect on the overall species composition at different
404 trophic levels, and may significantly affect entry and cycling of Se in seleniferous ecosystems.

405
406

407 **MATERIALS AND METHODS**

408

409 **Plant material**

410 *Astragalus bisulcatus* material was collected in the summer season (June-July) at Pine Ridge
411 Natural Area, a seleniferous site in Fort Collins, CO, USA. The leaf material used for X-ray
412 analysis was already described earlier (Freeman *et al.*, 2006a). After collection, some of the fresh
413 tissues were used for fungal endophyte culturing as described below. Samples for elemental
414 analysis were dried and analyzed for total Se and S, as described below. For μ XRF mapping and
415 μ XANES, the different plant parts from the field were flash frozen in liquid nitrogen, and the root
416 and stem were cross-sectioned to a thickness of 1mm using a new razor blade. Seeds were
417 surface-sterilized in a 20% bleach solution for 20 minutes, scarified by a concentrated sulfuric acid
418 treatment for 10 minutes, and rinsed five times for 10 minutes in sterile distilled water. Seedlings
419 were germinated on half-strength Murashige and Skoog medium (MS, Murashige and Skoog,
420 1962) plus B5 vitamins and 50 μ M sodium selenate, and then flash frozen in liquid nitrogen before
421 X-ray analysis.

422

423 **Fungal material**

424 Half of the surface-sterilized seeds germinated on MS medium showed evidence of colonization by
425 an endophytic fungus. This fungus was isolated and cultured on 0.5 strength Malt Extract Agar
426 (MEA, Difco) medium. Based on its morphology and ITS 1 and ITS 4 sequences (White *et al.*,
427 1990) the fungus was identified as a small-spored *Alternaria* species similar to other selenophilic
428 *Alternaria* species (Wangeline and Reeves, 2007). Endophytes inside leaf and stem cuttings were
429 recovered by first surface-sterilizing the tissue in 90% ethanol for 5 minutes, followed by treatment
430 with a 100% bleach solution for 5 minutes, before rinsing in sterile distilled water for 5 minutes.
431 Fungal endophytes were then isolated on MEA medium.

432

433 **Insect material**

434 Two different species of moth larvae were collected from *A. bisulcatus* while feeding on leaves at
435 the Pine Ridge field site. Some larvae were flash frozen in liquid nitrogen for microprobe
436 analyses, and some were kept alive in the laboratory feeding on their host, *A. bisulcatus* collected

437 from the field, until they pupated and eclosed. These adults were then flash frozen in liquid
438 nitrogen for X-ray analyses. The parasitoid wasp species that emerged from one of the moth
439 species pupae was also flash frozen for X-ray analyses.

440 To identify one of the Lepidoptera species, DNA was extracted using a Qiagen DNeasy
441 Blood and Tissue kit (Qiagen, Valencia, CA). Half an early-instar larva was ground, incubated at
442 56°C overnight in 100 µl of AE buffer, and DNA was then eluted following manufacturer
443 protocol. The DNA barcode region of the *cytochrome c oxidase I* (COI) gene (Hebert *et al.*,
444 2003a,b) was PCR amplified using an Eppendorf gradient Mastercycler 5331 (Eppendorf AG,
445 Hamburg, Germany). PCR reactions were performed using *TaKaRa Ex Taq* HS polymerase
446 (Takara Bio, Shiga, Japan) in a 50 µl final volume including the *Ex Taq* buffer and dNTP mixture.
447 The primers [LCO-1490 (5'-GGTCAACAAATCATAAAGATATTGG-3') and HCO-2198 (5'-
448 TAAACTTCAGGGTGACCAAAAATCA-3')] (Folmer, 1994) amplified a 658 bp DNA
449 segment. PCR on the Mastercycler involved a 3 minute denaturation step at 94°C , 32- 20 second
450 cycles at 94°C / 20 seconds at 50°C / 30 seconds at 72°C and a 5 minute extension step at 72°C.
451 Amplicons were purified using a Qiaquick PCR Purification Kit (Qiagen, Valencia, CA) and
452 sequenced at the University of Chicago Cancer Research Center. Contigs were assembled and
453 trimmed using Geneious Pro 5.3.4 (Biomatters Ltd., Auckland, New Zealand). The COI DNA
454 sequence was BLAST searched against the BOLD Systems animal identification (COI) species
455 barcode database (Ratnasingham and Hebert, 2007).

456

457 **Measurement of total Se and S concentration**

458 Before elemental analysis the biological material was rinsed with distilled water and dried for 48h
459 at 45°C. Samples were digested in nitric acid as described by Zarcinas *et al.* (1987). Inductively
460 coupled plasma atomic emission spectrometry (ICP-AES) was used to determine the
461 concentrations of Se and S in the acid digest (Fassel, 1978).

462

463 **X-ray spectroscopy studies**

464 Selenium distribution and speciation were investigated using µXRF and µXANES, respectively, as
465 described by Manceau *et al.* (2002) and Quinn *et al.* (2011b). Fresh, intact biological samples
466 were flash-frozen in liquid nitrogen and shipped on dry ice to the Advanced Light Source beamline

467 10.3.2 of the Lawrence Berkeley National Laboratory, Berkeley, CA for microprobe analyses
468 (Marcus *et al.*, 2004). Due to the time-intensive nature of μ XRF and μ XANES studies and the
469 limited beamtime available to individual research groups, one biological replicate was analyzed
470 unless stated otherwise. Frozen samples were placed on a -33°C Peltier stage to reduce radiation
471 damage caused by the X-ray beam. Micro-XRF elemental maps were recorded at 13 keV, using a
472 $15\ \mu\text{m}$ (H) x $6\ \mu\text{m}$ (V) beam spot size, $15\ \mu\text{m}$ x $15\ \mu\text{m}$ pixel size and 50 ms dwell time per pixel.
473 The chemical forms of Se in particular areas of interest were analyzed using Se K-edge XANES.
474 Micro-XRF maps and μ XANES spectra were recorded with a 7 element Ge solid state detector
475 (Canberra, ON, Canada). Spectra were deadtime corrected, pre-edge background subtracted, and
476 post-edge normalized using standard procedures (Kelly *et al.*, 2008). Red selenium (white line
477 energy set at 12660 eV) was used to calibrate each spectrum. Least square linear combination
478 (LSQ) analysis of Se XANES spectra was performed in the 12630-12850 eV range, through fitting
479 to a library of standard Se compounds. The error on the fit percentages of Se species was
480 estimated at $\pm 10\%$. Standards used were: Na_2SeO_4 , Na_2SeO_3 , SeCystine, SeMet purchased from
481 Sigma-Aldrich (St Louis, MO, USA), MeSeCys, gGMeSeCys, SeCysth, and SeGSH₂ purchased
482 from PharmaSe (Austin, TX, USA). SeCys was obtained by reducing SeCystine overnight at 25
483 $^{\circ}\text{C}$ in 100 mM sodium borohydride at a 1:1 molar ratio. Gray and red elemental Se standards were
484 provided by Amy Ryser and Dan Strawn. Data processing and analyses were performed using
485 custom LabVIEW (National Instruments, Austin, TX, USA) software programs available at the
486 beam line.

487

488 **ACKNOWLEDGMENTS**

489 We thank Scott Shaw from the University of Wyoming for identifying the ichneumon wasp.
490 Funding for these studies was provided by National Science Foundation grant # IOS-0817748 to
491 Elizabeth A. H. Pilon-Smits.

492

493 **LITERATURE CITED**

494 **Alford ÉR, Pilon-Smits EAH, Paschke MW** (2010) Metallophytes – a view from the
495 rhizosphere. *Plant Soil* **337**: 33-50

496 **Beath OA, Gilbert CS, Eppson HF** (1939a) The use of indicator plants in locating seleniferous
497 areas in Western United States. I. General. *Am J Bot* **26**: 257–269

498 **Beath OA, Gilbert CS, Eppson HF** (1939b) The use of indicator plants in locating seleniferous
499 areas in Western United States. II. Correlation studies by states. *Am J Bot* **26**: 296–315

500 **Boyd RS** (2007) The defense hypothesis of elemental hyperaccumulation: status, challenges and
501 new directions. *Plant Soil* **293**: 153–176

502 **Boyd RS** (2010) Heavy metal pollutants and chemical ecology: Exploring new frontiers. *J Chem*
503 *Ecol* **36**: 46–58

504 **de Souza MP, Pilon-Smits EAH, Lytle CM, Hwang S, Tai J, Honma, TSU, Yeh L, Terry N**
505 (1998) Rate-limiting steps in selenium assimilation and volatilization by Indian mustard. *Plant*
506 *Physiol* **117**: 1487–1494

507 **El Mehdawi AF, Quinn CF, Pilon-Smits EAH** (2011a) Effects of selenium hyperaccumulation
508 on plant–plant interactions: evidence for elemental allelopathy. *New Phytol* **191**: 120–131

509 **El Mehdawi AF, Quinn CF, Pilon-Smits EAH** (2011b) Selenium hyperaccumulators facilitate
510 selenium-tolerant neighbors via phytoenrichment and reduced herbivory. *Curr Biol* **21**: 1440-
511 1449

512 **El Mehdawi AF, Pilon-Smits EAH** (2012) Ecological aspects of plant selenium
513 hyperaccumulation. *Plant Biol* **14**: 1-10

514 **Fassel VA** (1978) Quantitative elemental analyses by plasma emission spectroscopy. *Science* **202**:
515 183–191

516 **Folmer O, Black M, Hoeh W, Lutz R, Vrijenhoek R** (1994) DNA primers for amplification of
517 mitochondrial *cytochrome c oxidase I* from diverse metazoan invertebrates. *Mol Marine Biol*
518 *Biotechnol* **3**: 294-299

519 **Freeman JL, Zhang LH, Marcus MA, Fakra S, Pilon-Smits EAH** (2006a) Spatial imaging,
520 speciation and quantification of selenium in the hyperaccumulator plants *Astragalus bisulcatus*
521 and *Stanleya pinnata*. *Plant Physiol* **142**: 124–134

522 **Freeman JL, Quinn CF, Marcus MA, Fakra S, Pilon-Smits EAH** (2006b) Selenium tolerant
523 diamondback moth disarms hyperaccumulator plant defense. *Curr Biol* **16**: 2181–2192

524 **Freeman JL, Lindblom SD, Quinn CF, Fakra S, Marcus MA, Pilon-Smits EAH** (2007)
525 Selenium accumulation protects plants from herbivory by Orthoptera via toxicity and
526 deterrence. *New Phytol* **175**: 490–500

527 **Freeman JL, Quinn CF, Lindblom SD, Klamper EM, Pilon-Smits EAH** (2009) Selenium
528 protects the hyperaccumulator *Stanleya pinnata* against black-tailed prairie dog herbivory in
529 native seleniferous habitats. *Am J Bot* **96**: 1075–1085

530 **Galeas ML, Zhang LH, Freeman JL, Wegner M, Pilon-Smits EAH** (2007) Seasonal
531 fluctuations of selenium and sulfur accumulation in selenium hyperaccumulators and related
532 nonaccumulators. *New Phytol* **173**: 517–525

533 **Galeas ML, Klamper EM, Bennett LE, Freeman JL, Kondratieff BC, Quinn CF, Pilon-Smits**
534 **EAH** (2008) Selenium hyperaccumulation reduced plant arthropod loads in the field. *New*
535 *Phytol* **177**: 715–724

536 **Gharieb MM, Wilkinson SC, Gadd GM** (1995) Reduction of selenium oxyanions by unicellular,
537 polymorphic and filamentous fungi: cellular location of reduced selenium and implications for
538 tolerance. *J Ind Microbiol* **14**: 300–311

539 **Grichanov IYA, Ovsyannikova EI** (2009) Pests: *Apamea sordens* *Hufn.* – Rustic shoulder-knot
540 moth. Interactive agricultural ecological atlas of Russia and neighboring countries: Economic
541 plants and their diseases, pests and weeds.
542 http://www.agroatlas.ru/pests/Apamea_sordens_en.htm

543 **Hanson B, Garifullina GF, Lindblom SD, Wangeline A, Ackley A, Kramer K, Norton AP,**
544 **Lawrence CB, Pilon-Smits EAH** (2003) Selenium accumulation protects *Brassica juncea*
545 from invertebrate herbivory and fungal infection. *New Phytol* **159**: 461–469

546 **Hanson B, Lindblom SD, Loeffler ML, Pilon-Smits EAH** (2004) Selenium protects plants from
547 phloem feeding aphids due to both deterrence and toxicity. *New Phytol* **162**: 655–662

548 **Hebert PD, Ratnasingham S, deWaard JR** (2003a) Barcoding animal life: cytochrome c oxidase
549 subunit 1 divergences among closely related species. *Proc Royal Soc London B* **270**: S96–S99

550 **Hebert PDN, Cywinska A, Ball SL, deWaard JR** (2003b) Biological identifications through
551 DNA barcodes. *Proc Royal Soc London B* **270**: 313–321

552 **Hunter WJ, Kuykendall LD** (2007) Reduction of selenite to elemental red selenium by
553 *Rhizobium sp.* strain B1. *Curr Microbiol* **55**: 344–349

554 **Hurd-Karrer AM, Poos FW** (1936) Toxicity of selenium-containing plants to aphids. *Science* **84**:
555 252

556 **Kelly SD, Hesterberg D, Ravel B** (2008) Analysis of soils and minerals using X-ray absorption
557 near-edge structure spectroscopy. *Methods of Soil Analysis, Part 5—Mineralogical Methods*
558 367

559 **Kinkle BK, Sadowsky MJ, Johnstone K, Koskinen WC** (1994) Tellurium and selenium
560 resistance in rhizobia and its potential use for direct isolation of *Rhizobium meliloti* from soil.
561 *Appl Environ Microbiol* **60**: 1674-1677

562 **Li H-F, McGrath SP, Zhao F-J** (2008) Selenium uptake, translocation and speciation in wheat
563 supplied with selenate or selenite. *New Phytol* **178**: 92–102

564 **Lindblom SD, Valdez-Barillas JR, Fakra SC, Marcus MA, Wangeline AL, Pilon-Smits EAH**
565 (2012) Influence of microbial associations on selenium localization and speciation in roots of
566 *Astragalus* and *Stanleya* hyperaccumulators. *Exp Environ Bot*, in press.
567 doi:10.1016/j.envexpbot.2011.12.011

568 **Losi ME, Frankenberger Jr WT** (1997) Reduction of selenium oxyanions by *Enterobacter*
569 *cloacae* SLD1a-1: Isolation and growth of the bacterium and its expulsion of selenium
570 particles. *Appl Environ Microbiol* **63**: 3079-3084

571 **Manceau A, Marcus MA, and Tamura N** (2002) Quantitative speciation of heavy metals and
572 soils and sediments by synchrotron X-ray techniques. In: P Fenter, NC Sturchio, eds,
573 Applications of synchrotron radiation in low-temperature geochemistry and environmental
574 science. *Reviews in Mineralogy and Geochemistry*, Vol. **49**. Mineralogical Society of
575 America, Washington, DC, pp 341-428

576 **Marcus MA, MacDowell AA, Celestre R, Manceau A, Miller T** (2004) Beamline 10.3.2 at
577 ALS: A hard X-ray microprobe for environmental and materials sciences. *J Synchrotron Radiat*
578 **11**: 239–247

579 **Murashige T, Skoog F** (1962) A revised medium for rapid growth and bioassays with tobacco
580 tissue culture. *Physiol Plant* **15**: 437-497

581 **Neuhierl B, Böck A** (1996) On the mechanism of selenium tolerance in selenium-accumulating
582 plants: Purification and characterization of a specific selenocysteine methyltransferase from
583 cultured cells of *Astragalus bisulcatus*. *Eur J Biochem* **239**, 235–238

584 **Pickering IJ, George GN, Van Fleet Stalder V, Chasteen TG, Prince RC** (1999) X ray
585 absorption spectroscopy of selenium-containing amino acids. *J Biol Inorg Chem* **6**: 791-794

586 **Pickering IJ, Prince RC, Salt DE, George GN** (2000) Quantitative chemically specific imaging
587 of selenium transformation in plants. *Proc Natl Acad Sci USA* **97**: 10717-10722

588 **Pilon-Smits EAH, Quinn CF** (2010) Selenium metabolism in plants. In: *Plant Cell Monographs*,
589 Vol 17, “Cell Biology of Metals and Nutrients”, R Hell, R Mendel, eds, pp 225-241

590 **Pilon-Smits EAH, Garifullina GF, Abdel-Ghany SE, Kato S-I, Mihara H, Hale KL,**
591 **Burkhead JL, Esaki N, Kurihara T, Pilon M** (2002) Characterization of a NifS-like
592 chloroplast protein from *Arabidopsis thaliana* – Implications for its role in sulfur and selenium
593 metabolism. *Plant Physiol* **130**: 1309-1318

594 **Powell JA, Opler PA** (2009) *Moths of western North America*. University of California Press,
595 Berkeley, 369 pp

596 **Quinn CF, Galeas ML, Freeman JL, Pilon-Smits EAH** (2007) Selenium: Deterrence, toxicity,
597 and adaptation. *Integr Environ Assess Manag* **3**: 460–462

598 **Quinn CF, Freeman JL, Galeas ML, Klamper EM, Pilon-Smits EAH** (2008) The role of
599 selenium in protecting plants against prairie dog herbivory: implications for the evolution of
600 selenium hyperaccumulation. *Oecologia* **155**: 267–275

601 **Quinn CF, Freeman JL, Reynolds RJB, Cappa JJ, Fakra SC, Marcus MA, Lindblom SD,**
602 **Quinn EK, Bennett LE, Pilon-Smits EAH** (2010) Selenium hyperaccumulation offers
603 protection from cell disruptor herbivores. *Plant Physiol* **153**: 1630–1652

604 **Quinn CF, Wyant K, Wangeline AL, Shulman J, Galeas ML, Valdez JR, Paschke MW,**
605 **Pilon-Smits EAH** (2011a) Selenium hyperaccumulation increases leaf decomposition rate in a
606 seleniferous habitat. *Plant Soil* **341**: 51-61

607 **Quinn CF, Prins CN, Freeman JL, Gross AM, Hantzis LJ, Reynolds RJB, Yang S, Covey PA,**
608 **Bañuelos GS, Pickering IJ, Pilon-Smits EAH** (2011b) Selenium accumulation in flowers and
609 its effects on pollination. *New Phytol* **192**: 727–737

610 **RalphsMH, Creamer R, Baucom D, Gardner DR, Welch SL, Graham JD, Hart C, Cook D,**
611 **Stegelmeier BL** (2007) Relationship between the endophyte *Embellisia sp.* and the toxic
612 alkaloid swainsonine in major locoweed species (*Astragalus* and *Oxytropis*). *J Chem Ecol* **34**:
613 32-28

614 **Ratnasingham S, Herbert PDN** (2007) BOLD: The Barcode of Life Data System
615 (www.barcodinglife.org). Mol Ecol Notes **7**: 355-364

616 **Robinson GS, Ackery PR, Kitching IJ, Becaloni GW, Hernández LM** (2010) HOSTS – A
617 Database of the World's Lepidopteran Hostplants. Natural History Museum, London.
618 <http://www.nhm.ac.uk/hosts>

619 **Sarles WB, McCaffrey JC, Mickelson, MN** (1935) Studies on the classification and
620 differentiation of the rhizobia. J Bacteriol **29**: 74-75

621 **Sors TG, Ellis DR, Salt DE** (2005) Selenium uptake, translocation, assimilation and metabolic
622 fate in plants. Photosynth Res **86**: 373–389

623 **Stadtman TC** (1990) Selenium biochemistry. Annu Rev Biochem **59**: 111-127

624 **Vickerman DB, Shannon MC, Bañuelos GS, Grieve CM, Trumble JT** (2002) Evaluation of
625 *Atriplex* lines for selenium accumulation, salt tolerance and suitability for a key agricultural
626 insect pest. Environ Poll **120**: 463–473

627 **Wangeline AL, Reeves FB** (2007) Two new *Alternaria* species from selenium-rich habitats in the
628 Rocky Mountain Front Range. Mycotaxon **99**: 83-89

629 **Wangeline AL, Valdez JR, Lindblom SD, Bowling KL, Reeves FB, Pilon-Smits EAH** (2011)
630 Characterization of rhizosphere fungi from selenium hyperaccumulator and
631 nonhyperaccumulator plants along the eastern Rocky Mountain Front Range. Am J Bot **98**:
632 1139-1147

633 **White TJ, Bruns T, Lee S, Taylor L** (1990) Amplification and direct sequencing of fungal
634 ribosomal RNA genes for phylogenetics. In: Innis MA *et al.*, eds. PCR Protocols: a guide to
635 methods and applications. Acad Press, San Diego, pp 315-322

636 **Wilson JK, Chin CH** (1947) Symbiotic studies with isolates from nodules of species of
637 *Astragalus*. Soil Sci **63**: 119-127

638 **Wu L, Emberg A, Biggar JA** (1994) Effects of elevated selenium concentration on selenium
639 accumulation and nitrogen-fixation symbiotic activity of *Melilotus indica* L. Ecotox Environ
640 Saf **27**: 50-63

641 **Zarcinas BA, Cartwright B, Spouncer LR** (1987) Nitric acid digestion and multi element
642 analysis of plant material by inductively coupled plasma spectrometry. Commun Soil Sci
643 Plant **18**: 131–146

644

645 **FIGURE LEGENDS**

646

647 **(COLOR, FOR ONLINE VERSION)**

648

649 **Figure 1.** (A) X-ray fluorescence (μ XRF) map showing distribution of Se (in red), Ca (in green)
650 and iron (in blue) in a cross-section of an *A. bisulcatus* taproot. (B) Se speciation in the tap root as
651 determined by X-ray absorption near edge structure (XANES) spectroscopy at the locations
652 indicated in panel A by circles. (C) Distribution of Se (in red), Ca (in green) and Zn (in pink) in a
653 lateral root with nodule. (D) Se speciation in the tip of the lateral root (locations shown as white
654 circles in C). (E) Se speciation in the nodule (locations shown as white circles in C).

655

656 **Figure 2.** (A) μ XRF map showing distribution of Se (in red), Ca (in green) and iron (in blue) in a
657 cross-section of an *A. bisulcatus* stem. (B) composition of Se in the stem as determined by
658 XANES. (C) μ XRF map showing distribution of Se (in red) and S (in green) in a leaflet of *A.*
659 *bisulcatus* (inset was mapped at higher resolution) (D) Se composition in the leaflet as determined
660 by XANES. White circles represent locations where XANES scans were performed to determine
661 Se speciation.

662

663 **Figure 3.** (A) μ XRF map showing distribution of Se (in red), K (green) and Zn (blue) in larva of
664 *Apamea sordens* collected from *A. bisulcatus*. (B) Selenium composition in larval tissue (white
665 circles in A) as determined by XANES. (C) Se composition in larval hindgut (black circle in A).
666 (D) Photograph of adult. (E) μ XRF map showing distribution of Se (in red) Zn (green) and K
667 (blue) in the adult moth. (F) Composition of Se in the adult moth as determined by XANES (white
668 circles in E). (G) Photograph of parasitic wasp from *Apamea sordens*. (H) μ XRF map showing
669 distribution of Se (in red) . Zmn (green) and Ca (blue) in the parasitic wasp. (I) Se composition in
670 the wasp at the locations indicated by white circles in I, and (J) Se composition in the wasp at the
671 location indicated by the black circle in I, as determined by XANES.

672

673 **Figure 4.** (A) Photograph of larva of gelechiid moth, collected from *A. bisulcatus*. (B) μ XRF map
674 showing distribution of Se (in red), Zn (in green) and Ca (in blue) in the larva's anterior. (C)

675 Composition of Se in the larval tissues (white circles in B) as determined by XANES. (D)
676 Photograph of adult moth. (E) μ XRF map showing distribution of Se (in red), Zn (in green) and
677 Ca (in blue) in the adult's posterior. (F) Composition of Se in the adult moth's tissues (white
678 circles in E), as determined by XANES.

679

680 **Figure 5.** (A) Photograph of *A. bisulcatus* flower. (B) μ XRF map showing distribution of Se (in
681 red) and Ca (in green) in the petals of the flower. (C) μ XRF map showing distribution of Se (in
682 red) and Ca (in green) in the pistil and stamen of the flower, and in the seed pod (inset). (D)
683 Composition of Se in all floral parts, as determined by XANES. Circles in B and C show where
684 XANES scans were performed to determine Se composition.

685

686 **Figure 6.** (A) Photograph of an *A. bisulcatus* seed. (B) μ XRF map showing distribution of Se
687 (red), Zn (green) and Ca (blue) in the seed. (C) Se composition in the embryo within the seed
688 (white circles in B) as determined by XANES. (D) Photograph of fungal endophyte emerging from
689 germinating *A. bisulcatus* seed. (E) μ XRF map showing distribution of Se (red) and Ca (green) in
690 endophyte-containing *A. bisulcatus* seed and in the mycelium of the emerging endophytic fungus
691 (inset). (F) Se composition in fungal mycelium growing out from the seed (white circles in E), and
692 (G) Se composition in the endophyte-containing seed (black circle in E) as determined by XANES.

693

694 **Figure 7.** (A) Photograph of *A. bisulcatus* seedling, with empty seed coat to its left. (B) μ XRF
695 map showing distribution of Se (in red) and Ca (in green) in 24h old *A. bisulcatus* seedling. (C) Se
696 composition in endophyte-containing seedling 24 hours after germination, as determined by
697 XANES at the points indicated by circles in panel B. (D) μ XRF map showing Se (red) and Ca
698 (green) distribution in 5d old *A. bisulcatus* seedling. (E) Se composition in the cotyledons of 5d old
699 endophyte-containing seedling (white circle in D). (F) Se composition in the root of 5d old
700 endophyte-containing seedling (black circle in D) as determined by XANES.

701

702 **Figure 8.** Schematic overview of Se uptake, translocation and speciation in different *A. bisulcatus*
703 organs, and the associated ecological interactions.

704

705 **(BLACK & WHITE, FOR PAPER VERSION)**

706

707 **Figure 1.** (A) X-ray fluorescence (μ XRF) map showing Se distribution (in white) in a cross-
708 section of an *A. bisulcatus* taproot. (B) Se speciation in the tap root as determined by X-ray
709 absorption near edge structure (XANES) spectroscopy at the locations indicated in panel A by
710 circles. (C) Se distribution (in white) in a lateral root with nodule. (D) Se speciation in the lateral
711 root (locations shown as white circles in C). (E) Se speciation in the nodule (locations shown as
712 black circles in C).

713

714 **Figure 2.** (A) μ XRF map showing Se distribution (in white) in a cross-section of an *A. bisulcatus*
715 stem. (B) composition of Se in the stem as determined by XANES. (C) μ XRF map showing Se
716 distribution (in white) in a leaflet of *A. bisulcatus*; the inset was mapped at a higher resolution. (D)
717 Se composition in the leaflet as determined by XANES. White circles represent areas where
718 XANES scans were performed to determine Se speciation.

719

720 **Figure 3.** (A) μ XRF map showing Se distribution (in white) in larva of *Apamea sordens* collected
721 from *A. bisulcatus*. (B) Selenium composition in larval tissue (white circles in A) as determined by
722 XANES. (C) Se composition in larval hindgut (black circle in A). (D) Photograph of adult. (E)
723 μ XRF map showing Se distribution (in white) in the adult moth. (F) Composition of Se in the adult
724 moth's hindgut as determined by XANES (circles in E). (G) Photograph of parasitic wasp from
725 *Apamea sordens*. (H) μ XRF map showing Se distribution (in white) in the parasitic wasp. (I) Se
726 composition in the wasp at the locations indicated by white circles in I, and (J) Se composition in
727 the wasp at the location indicated by the black circle in I, as determined by XANES.

728

729 **Figure 4.** (A) Photograph of larva of gelechiid moth, collected from *A. bisulcatus*. (B) μ XRF map
730 showing Se distribution (in white) in the larva's anterior. (C) Composition of Se in the larval
731 tissues (black circles in B) as determined by XANES. (D) Photograph of adult moth. (E) μ XRF
732 map showing Se distribution (in white) in the adult's posterior. (F) Composition of Se in the adult
733 moth's tissues (black circles in E), as determined by XANES.

734

735 **Figure 5.** (A) Photograph of *A. bisulcatus* flower. (B) μ XRF map showing Se distribution (in
736 white) in the petals of the flower. (C) μ XRF map showing Se distribution (in white) in the pistil
737 and stamen of the flower, and in the seed pod (inset). (D) Composition of Se in all floral parts, as
738 determined by XANES. Circles in B and C show where XANES scans were performed to
739 determine Se composition.

740
741 **Figure 6.** (A) Photograph of an *A. bisulcatus* seed. (B) μ XRF map showing Se distribution (in
742 white) in the seed. (C) Se composition in the embryo within the seed (white circles in B) as
743 determined by XANES. (D) Photograph of fungal endophyte emerging from germinating *A.*
744 *bisulcatus* seed. (E) μ XRF map showing Se distribution (in white) in endophyte-containing *A.*
745 *bisulcatus* seed and in the mycelium of the emerging endophytic fungus (inset). (F) Se composition
746 in fungal mycelium growing out from the seed (white circles in E), and (G) Se composition in the
747 endophyte-containing seed (black circle in E) as determined by XANES.

748
749 **Figure 7.** (A) Photograph of *A. bisulcatus* seedling, with empty seed coat to its left. (B) μ XRF
750 map showing distribution of Se (in white in 24h old *A. bisulcatus* seedling. (C) Se composition in
751 endophyte-containing seedling 24 hours after germination, as determined by XANES at the points
752 indicated by circles in panel B. (D) μ XRF map showing Se (in white) distribution in 5d old *A.*
753 *bisulcatus* seedling. (E) Se composition in the cotyledons of 5d old endophyte-containing seedling
754 (white circle in D). (F) Se composition in the root of 5d old endophyte-containing seedling (black
755 circle in D) as determined by XANES.

756
757 **Figure 8.** Schematic overview of Se uptake, translocation and speciation in different *A. bisulcatus*
758 organs, and associated ecological interactions.

759

1 **Table I:** Selenium and sulfur concentration (mg kg^{-1} DW) in different organs and floral
 2 parts of *A. bisulcatus*. Values shown for organs and floral parts were from different
 3 plants. Shown are means +/- standard error of the mean; n = 6 except for roots and stems
 4 where n = 3. Letters indicate significant difference among plant organs for each element
 5 using Tukey-Kramer HSD ($P < 0.05$)

	<u>Selenium</u>	<u>Sulfur</u>
<u>Organs</u>		
Roots	704 ± 236 ^a	3388 ± 1270 ^b
Stems	4557 ± 1233 ^b	3622 ± 1735 ^b
Leaves	3045 ± 927 ^b	16254 ± 1709 ^a
Flowers	4661 ± 1243 ^b	6733 ± 927 ^b
<u>Floral parts</u>		
Sepals	6095 ± 3637 ^a	9355 ± 911 ^{ac}
Petals	4163 ± 2504 ^a	6223 ± 802 ^{ab}
Stamens	1817 ± 1239 ^a	5614 ± 1126 ^{ab}
Pistils	3575 ± 2290 ^a	3950 ± 520 ^b
Immature seeds	3153 ± 1356 ^a	11837 ± 1486 ^c

6

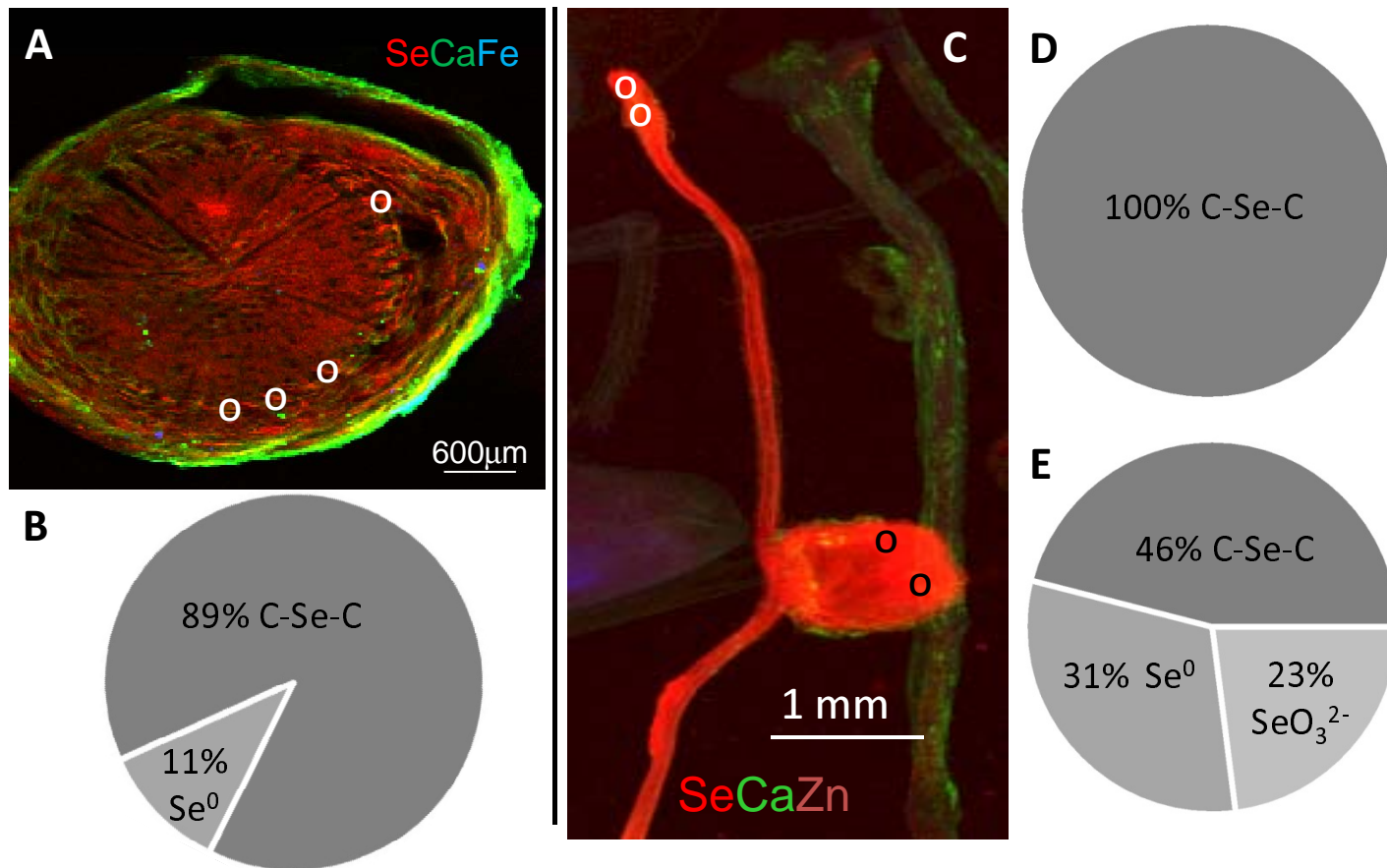


Figure 1. (A) X-ray fluorescence (μ XRF) map showing distribution of Se (in red), Ca (in green) and iron (in blue) in a cross-section of an *A. bisulcatus* taproot. (B) Se speciation in the tap root as determined by X-ray absorption near edge structure (XANES) spectroscopy at the locations indicated in panel A by circles. (C) Distribution of Se (in red), Ca (in green) and Zn (in pink) in a lateral root with nodule. (D) Se speciation in the tip of the lateral root (locations shown as white circles in C). (E) Se speciation in the nodule (locations shown as white circles in C).

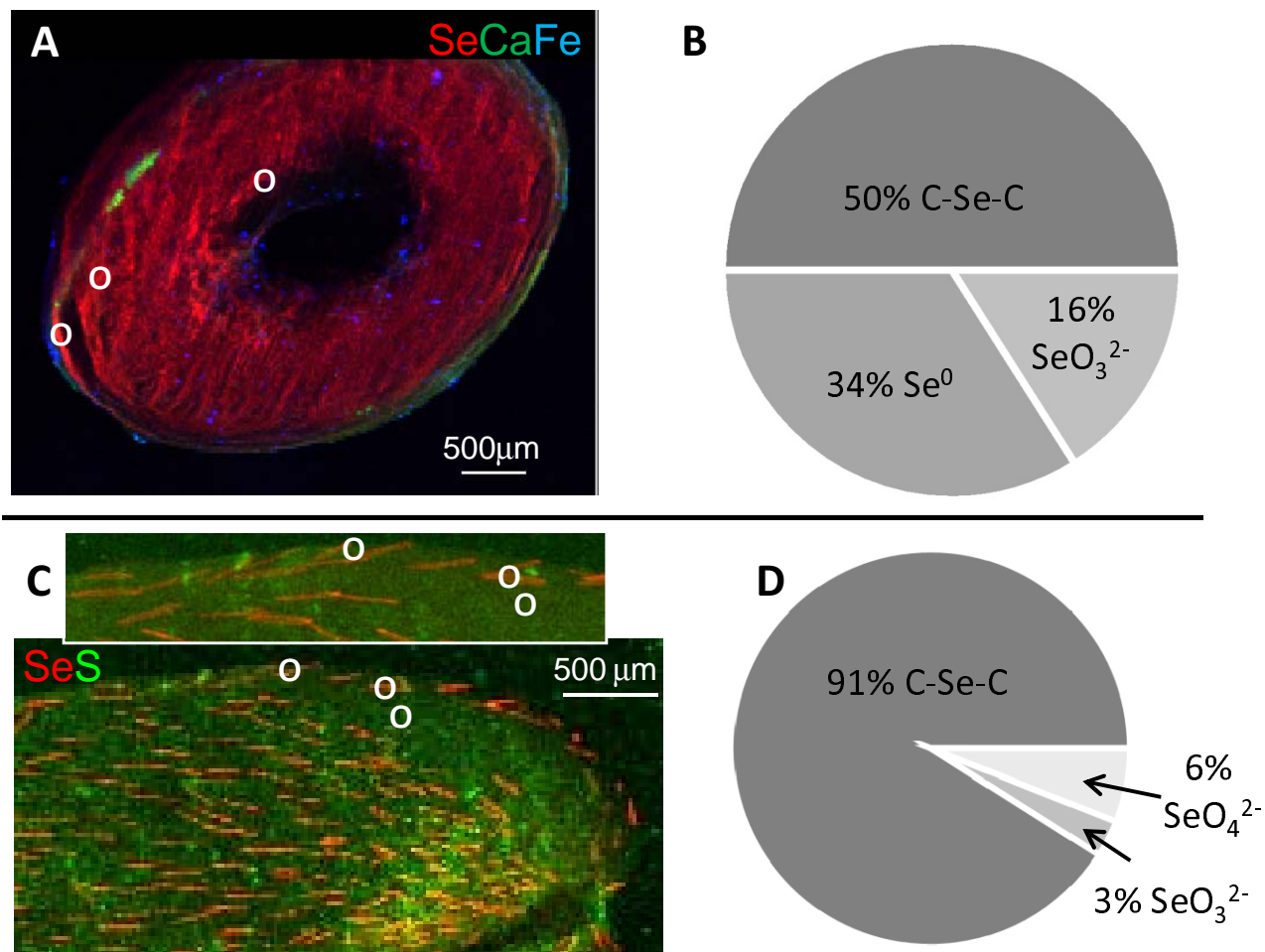


Figure 2. (A) μXRF map showing distribution of Se (in red), Ca (in green) and iron (in blue) in a cross-section of an *A. bisulcatus* stem. (B) composition of Se in the stem as determined by XANES. (C) μXRF map showing distribution of Se (in red) and S (in green) in a leaflet of *A. bisulcatus* (inset was mapped at higher resolution) (D) Se composition in the leaflet as determined by XANES. White circles represent locations where XANES scans were performed to determine Se speciation.

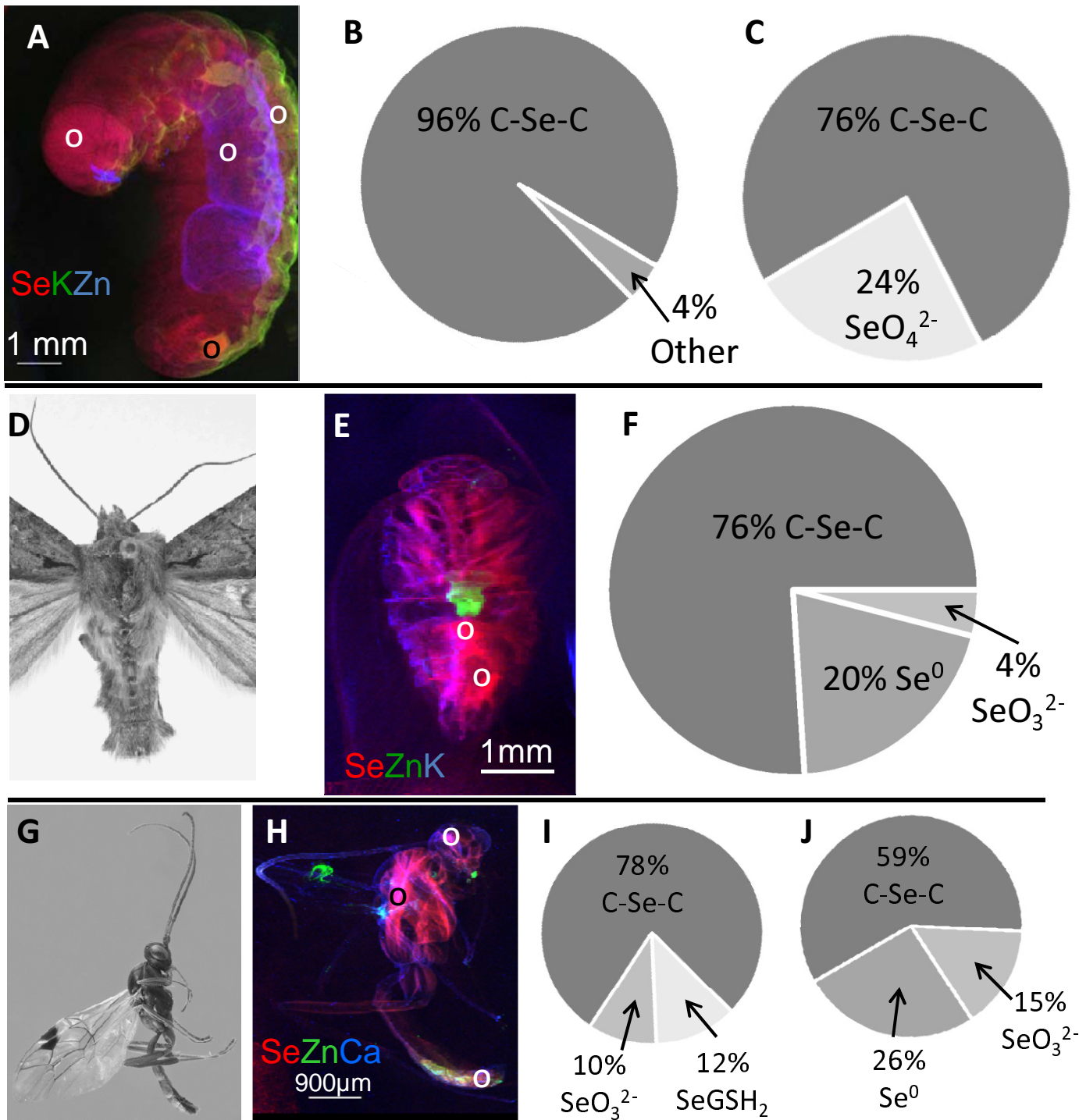


Figure 3. (A) μ XRF map showing distribution of Se (in red), K (green) and Zn (blue) in larva of *Apamea sordens* collected from *A. bisulcatus*. (B) Selenium composition in larval tissue (white circles in A) as determined by XANES. (C) Se composition in larval hindgut (black circle in A). (D) Photograph of adult. (E) μ XRF map showing distribution of Se (in red) Zn (green) and K (blue) in the adult moth. (F) Composition of Se in the adult moth as determined by XANES (white circles in E). (G) Photograph of parasitic wasp from *Apamea sordens*. (H) μ XRF map showing distribution of Se (in red) . Zn (green) and Ca (blue) in the parasitic wasp. (I) Se composition in the wasp at the locations indicated by white circles in I, and (J) Se composition in the wasp at the location indicated by the black circle in I, as determined by XANES.

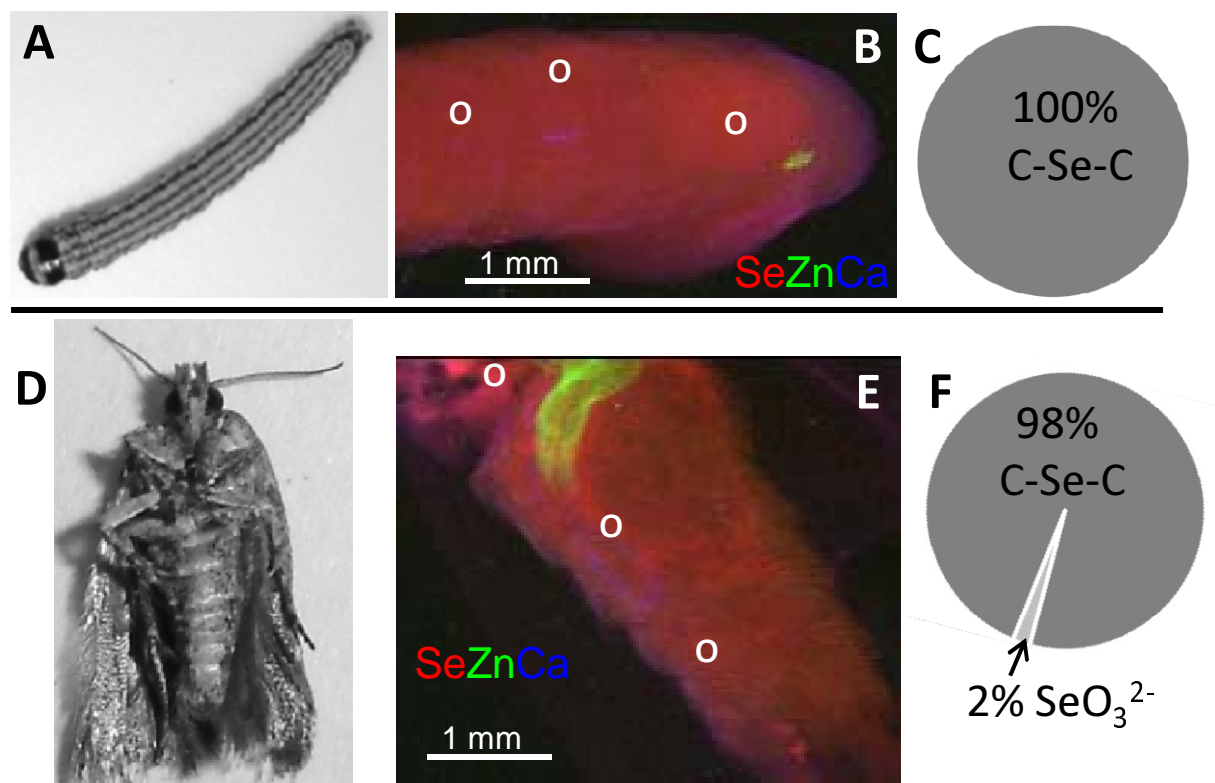


Figure 4. (A) Photograph of larva of gelechiid moth, collected from *A. bisulcatus*. (B) μ XRF map showing distribution of Se (in red), Zn (in green) and Ca (in blue) in the larva's anterior. (C) Composition of Se in the larval tissues (white circles in B) as determined by XANES. (D) Photograph of adult moth. (E) μ XRF map showing distribution of Se (in red), Zn (in green) and Ca (in blue) in the adult's posterior. (F) Composition of Se in the adult moth's tissues (white circles in E), as determined by XANES.

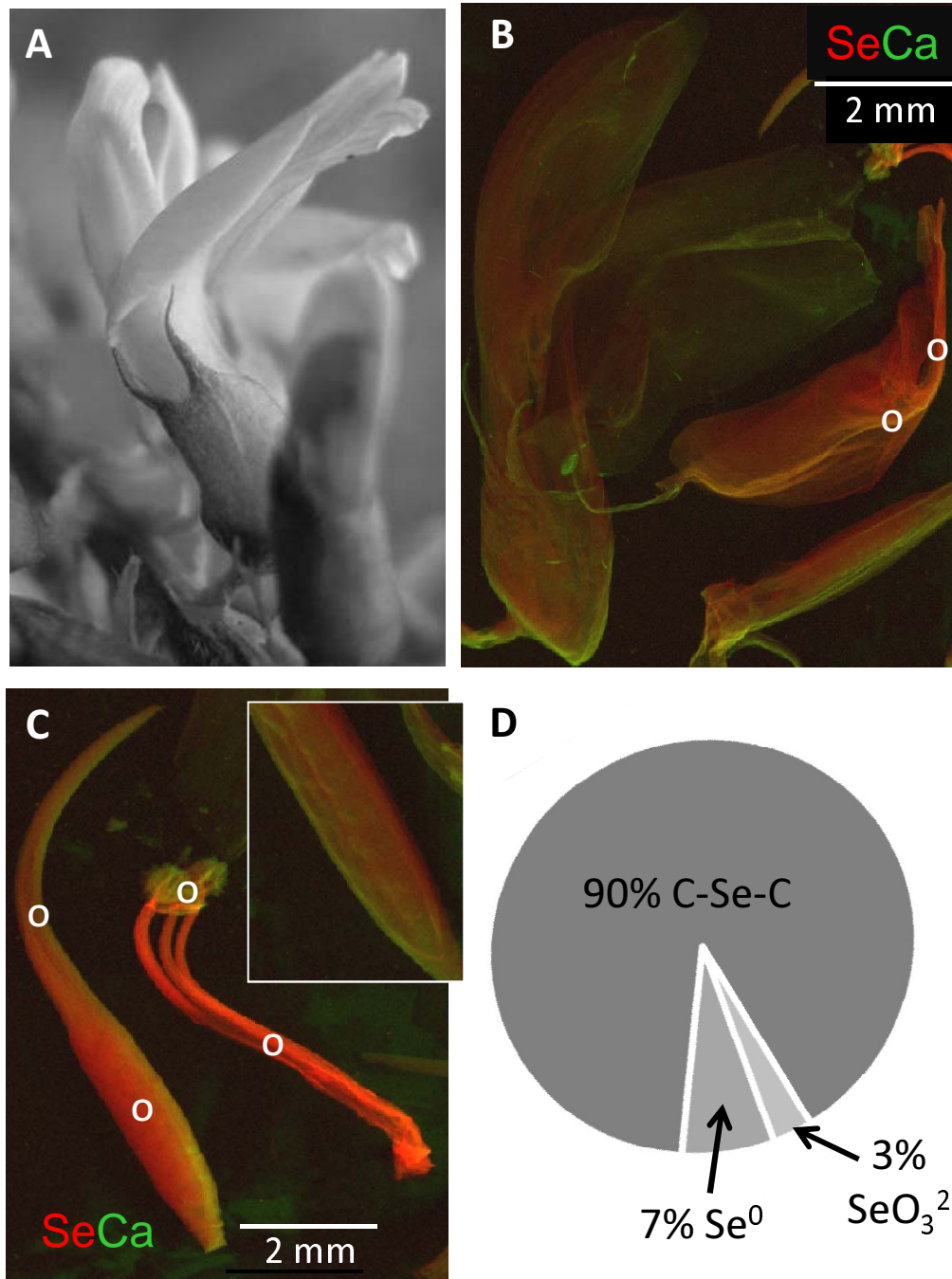


Figure 5. (A) Photograph of *A. bisulcatus* flower. (B) μ XRF map showing distribution of Se (in red) and Ca (in green) in the petals of the flower. (C) μ XRF map showing distribution of Se (in red) and Ca (in green) in the pistil and stamen of the flower, and in the seed pod (inset). (D) Composition of Se in all floral parts, as determined by XANES. Circles in B and C show where XANES scans were performed to determine Se composition.

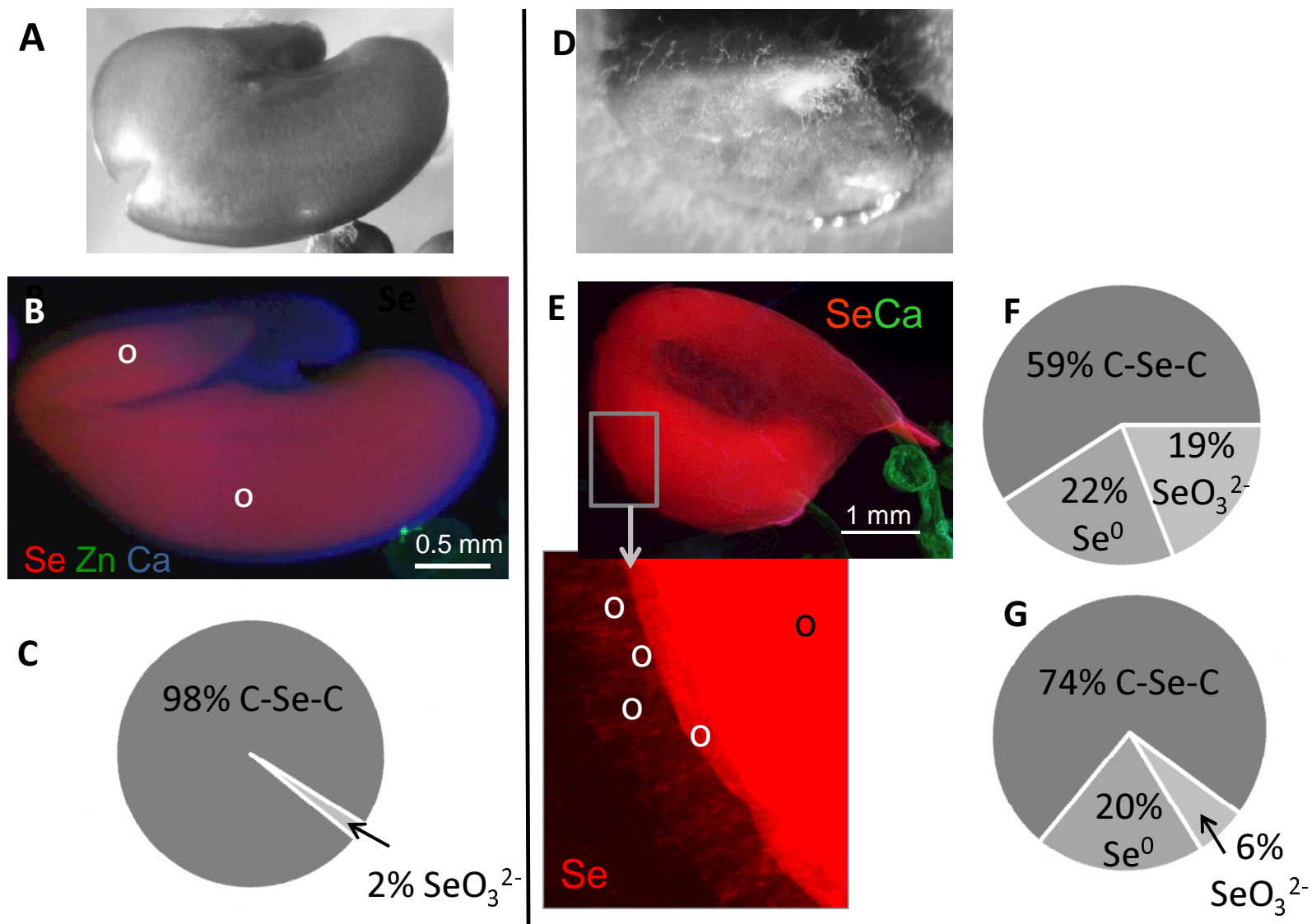


Figure 6. (A) Photograph of an *A. bisulcatus* seed. (B) μ XRF map showing distribution of Se (red), Zn (green) and Ca (blue) in the seed. (C) Se composition in the embryo within the seed (white circles in B) as determined by XANES. (D) Photograph of fungal endophyte emerging from germinating *A. bisulcatus* seed. (E) μ XRF map showing distribution of Se (red) and Ca (green) in endophyte-containing *A. bisulcatus* seed and in the mycelium of the emerging endophytic fungus (inset). (F) Se composition in fungal mycelium growing out from the seed (white circles in E), and (G) Se composition in the endophyte-containing seed (black circle in E) as determined by XANES.

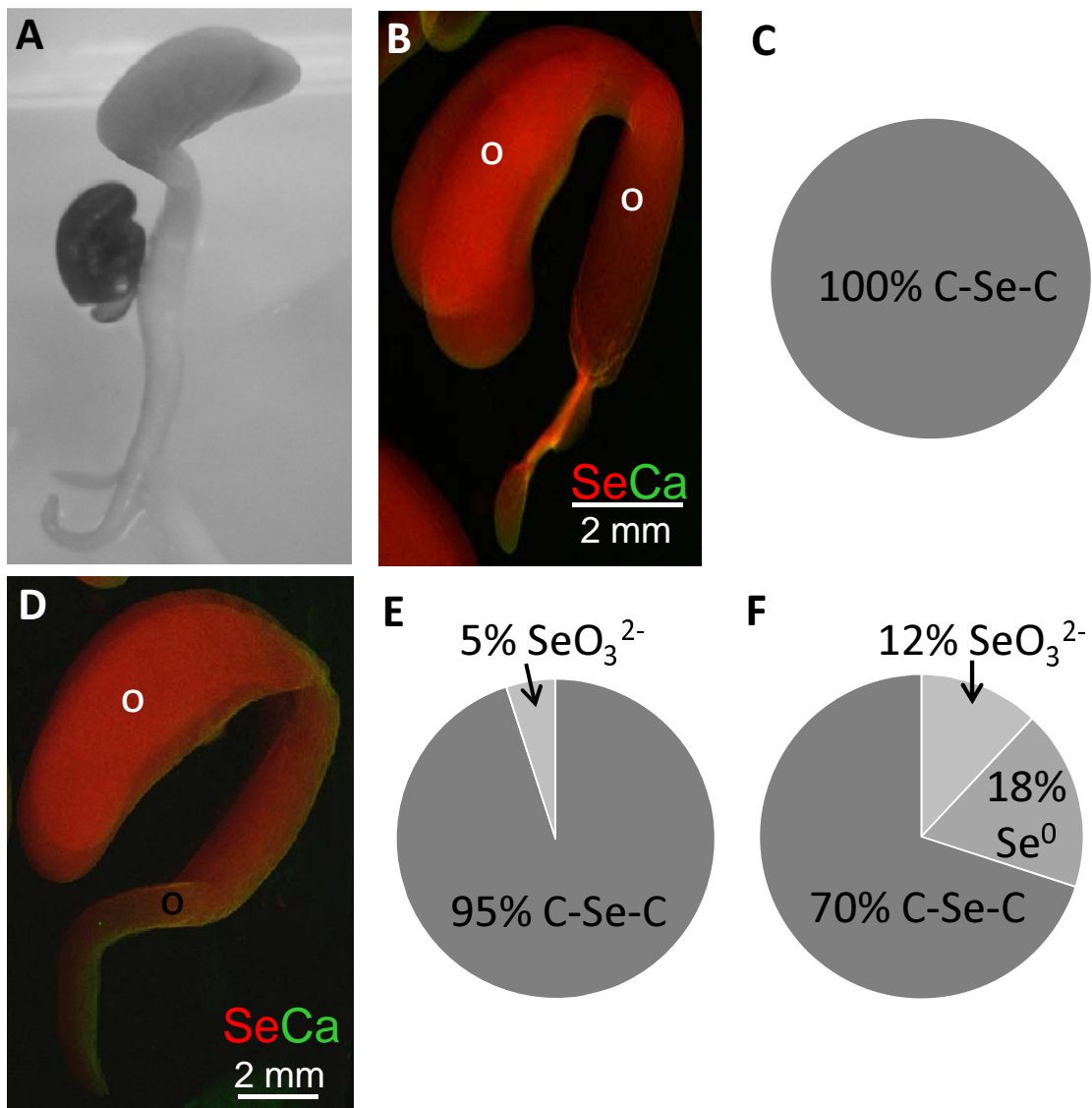


Figure 7. (A) Photograph of *A. bisulcatus* seedling, with empty seed coat to its left. (B) μ XRF map showing distribution of Se (in red) and Ca (in green) in 24h old *A. bisulcatus* seedling. (C) Se composition in endophyte-containing seedling 24 hours after germination, as determined by XANES at the points indicated by circles in panel B. (D) μ XRF map showing Se (red) and Ca (green) distribution in 5d old *A. bisulcatus* seedling. (E) Se composition in the cotyledons of 5d old endophyte-containing seedling (white circle in D). (F) Se composition in the root of 5d old endophyte-containing seedling (black circle in D) as determined by XANES.

Selenium Uptake, Translocation and Speciation

Flowers accumulate primarily C-Se-C (90%), with small fractions of elemental Se (7%) and SeO_3^{2-} (3%)

91% of leaf Se is C-Se-C; the remainder is SeO_4^{2-} (6%) and SeO_3^{2-} (3%)

50% of Se in the stem is C-Se-C; the remainder is elemental Se (34%) and SeO_3^{2-} (16%)

C-Se-C makes up 89% of Se in roots; the remaining 11% is elemental Se

Soil Se is taken up, presumably as SeO_4^{2-}

Ecological Interactions

Two apparently Se-tolerant moth species can forage on Se-rich *A. bisulcatus* leaves. Both accumulate primarily C-Se-C. One of the moths is parasitized by a wasp, which also accumulates C-Se-C and may be Se-tolerant.

An apparently Se-tolerant endophytic fungus is found in seeds and throughout the mature plant. It produces high levels of elemental Se (22%), which may affect plant Se metabolism.

Nitrogen-fixing bacterial symbiont in root nodules may affect plant Se speciation, since nodules contain higher levels of elemental Se than the root (up to 31%).

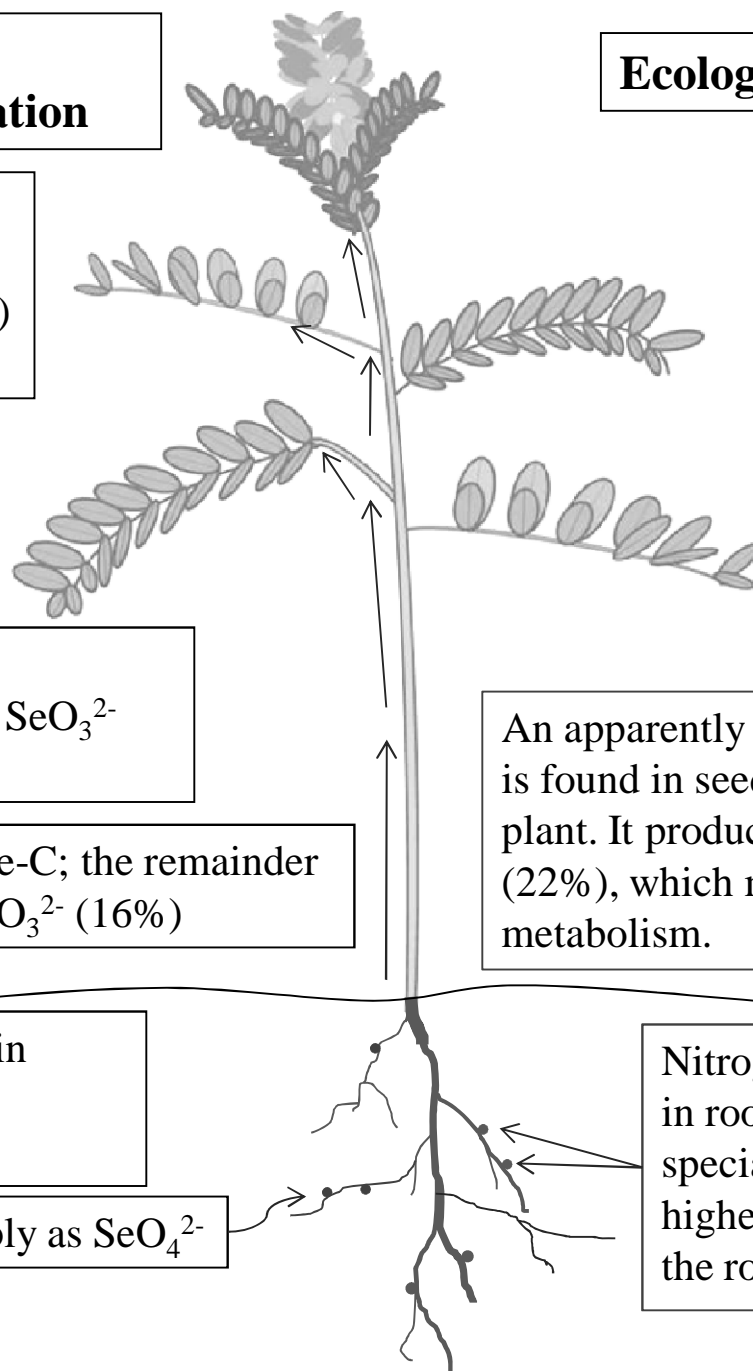


Figure 8.

Schematic overview of Se uptake, translocation and speciation in different *A. bisulcatus* organs, and associated ecological interactions.